ACS APPLIED MATERIALS & INTERFACES
Research Article
www.acsami.org

Efficient Charge Injection in p-Type Polymer Field-Effect Transistors with Low-Cost Molybdenum Electrodes through V_2O_5 Interlayer

Kang-Jun Baeg,[†] Gwang-Tae Bae,[‡] and Yong-Young Noh*,[‡]

[‡]Department of Energy and Materials Engineering, Dongguk University, 26 Pil-dong, 3-ga, Jung-gu, Seoul 100-715, Republic of Korea

[†]Nano Carbon Materials Research Group, Korea Electrotechnology Research Institute (KERI), 12 Bulmosan-ro 10 beon-gil, Changwon, Gyeongsangnam-do 642-120, Republic of Korea

Supporting Information

ABSTRACT: Here we report high-performance polymer OFETs with a low-cost Mo source/drain electrode by efficient charge injection through the formation of a thermally deposited V_2O_5 thin film interlayer. A thermally deposited V_2O_5 interlayer is formed between a regioregular poly(3-hexylthiophene) (rr-P3HT) or a p-type polymer semiconductor containing dodecyl-substituted thienylenevinylene (TV) and dodecylthiophene (PC12TV12T) and the Mo source/drain electrode. The P3HT or PC12TV12T OFETs with the bare Mo electrode exhibited lower charge carrier mobility than those with Au owing to a large barrier height for hole injection (0.5–1.0 eV). By forming the V_2O_5 layer, the P3HT or PC12TV12T OFETs with V_2O_5 on the Mo electrode exhibited charge carrier mobility comparable to that of a pristine Au electrode. Best P3HT or PC12TV12T OFETs with 5 nm thick V_2O_5 on Mo electrode show the charge carrier mobility of 0.12 and 0.38 $cm^2/(V\ s)$, respectively. Ultraviolet photoelectron spectroscopy results exhibited the work-function of the Mo electrode progressively changed from 4.3 to 4.9 eV with an increase in V_2O_5 thickness from 0 to 5 nm, respectively. Interestingly, the V_2O_5-deposited Mo exhibits comparable R_c to Au, which mainly results from the decreased barrier height for hole carrier injection from the low-cost metal electrode to the frontier molecular orbital of the p-type polymer semiconductor after the incorporation of the transition metal oxide hole injection layer, such as V_2O_5. This enables the development of large-area, low-cost electronics with the Mo electrodes and V_2O_5 interlayer.

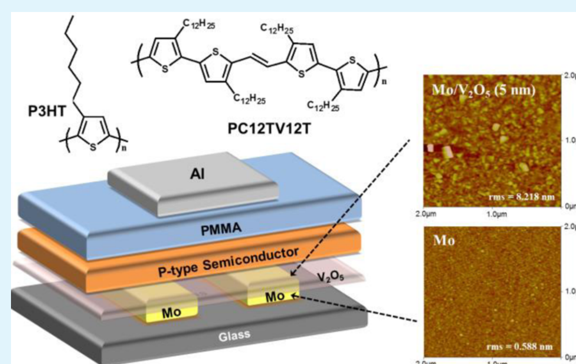

KEYWORDS: *organic field-effect transistors, vanadium pentoxide, contact resistance, interlayer, molybdenum, low-cost electrode*

1. INTRODUCTION

Over the past decade, organic field-effect transistors (OFETs) have attracted tremendous research interests for realizing flexible/stretchable and low-cost/large-area electronics and optoelectronics.[1] We expect the realization of soft electronics based on organic semiconductors by successful development of high-performance materials including semiconductors, electrodes, and dielectrics; interface engineering between semiconductors and dielectrics or between semiconductors and source/drain charge injection electrodes;[2,3] and optimization of the fabrication processes with cost-effective graphic art printing techniques.[4] Most importantly, relatively low charge carrier mobility of the active semiconductor layer has rendered it difficult to use OFETs in a variety of high-end potential applications, such as thin-film transistor (TFT) backplane of active matrix displays, electronic circuit/logic in microprocessors, and radio frequency identification tags, because these applications typically need a high charge carrier mobility for a fast switching speed. Although its progress has been delayed for some time, recently, state-of-the-art p-type and n-type organic (including polymer) semiconductors have been designed to achieve high charge carrier mobilities generally exceeding 1 $cm^2/(V\ s)$[5,6] and even record high mobility exceeding 10 $cm^2/(V\ s)$ with polymers[7] by optimizing the molecular design and by increasing the molecular weight, followed by improving the chemical synthesis and device fabrication process.

The maximum transit frequency (f_T) of the OFETs with an apparent device mobility (μ_{app}) of 1 $cm^2/(V\ s)$ and lateral dimensions of channel length $L = 1\ \mu m$ can achieve up to ∼100 MHz at a supplied voltage of 30 V.[8] However, this estimate is only a theoretical value obtained without considering the parasitic overlap capacitances and contact resistance (R_c) at such a short L scale. When L of the OFETs is further reduced to the submicrometer scale, R_c has to be seriously taken into account because R_c is close to or higher than the channel resistance (R_{ch}) in the OFETs. It causes significant degradation of μ_{app} below the intrinsic mobility (μ_i) of the organic semiconductors, as shown in eq 1[9]

Received: April 15, 2013
Accepted: June 4, 2013
Published: June 4, 2013

ACS Publications © 2013 American Chemical Society

$$\mu_{app} \approx \mu_i \left[1 - \left(\frac{\mu_i C_i W R_c (V_g - V_{Th})}{L + \mu_i C_g W R_c (V_g - V_{Th})} \right)^2 \right] \quad (1)$$

where W, C_g, V_g, and V_{Th} are the channel width, gate dielectric capacitance, gate voltage, and threshold voltage, respectively. Therefore, it is imperative to use Ohmic contact electrodes for efficient charge carrier injection from the source/drain electrodes to the semiconductor active channel, thereby obtaining the optimum μ_{app} close to the μ_i value.

High-performance p-type OFETs have mostly been built with expensive gold (Au) electrodes owing to their inherently high work function (Φ), excellent electrical conductivity, and environmental stability.[10] As an alternative to the expensive noble metal, low-cost metal electrodes, such as copper (Cu) or molybdenum (Mo), as well as conducting polymers[11] and nanocarbon materials,[12,13] have been used in p-type OFETs. Although these conducting polymers and nanocarbon materials typically exhibit comparable or even better charge injection properties than Au in OFETs,[14] they exhibit a relatively low electrical conductivity of <1000 S/cm (for conducting polymers and solution-processed nanocarbon inks and pastes) when compared with metal electrodes, which could cause a serious problem of decreasing the signal processing time because of the parasitic resistance−capacitance (RC) time delay in the integrated circuit and limitation to an achievable panel size and slow image frame time in the active matrix displays. Notably, many industrial companies are known to use Mo as electrodes for the TFT backplane in large-area flat panel displays owing to its high electrical conductivity as well as reasonable price. Mo is a transition metal with a low electrical resistivity of $\sim 5 \times 10^{-6}$ Ω cm, and it is available at a much lower price (∼26 $/kg) when compared with Au (∼51 000 $/kg). For low-cost and large-area organic electronics and optoelectronics, therefore, Mo is considered as a promising electrode material. However, a method for achieving efficient charge injection properties with Mo should be developed to realize high-performance OFETs because Φ of Mo is not well-matched with the typical energetic levels of organic semiconductors.

Many low-cost metal electrodes such as Mo have a relatively low Φ of 4.3−4.6 eV, which generally causes a large barrier height for hole carrier injection from the source/drain electrodes in OFETs because the highest occupied molecular orbital (HOMO) energetic levels of the typical conjugated molecules used as the active layer are in the range of 4.5−6.5 eV. In addition, a HOMO level of below 5.0 eV protects the conjugated molecules from unwanted interaction with the oxygen and moisture in the air and provides a better ambient stability. Moreover, interfacial dipoles (Δ) formed as organic molecules are adsorbed onto the metal electrode, leading to further increase in the barrier height by shifting the vacuum level alignment between the semiconductor and the contact electrodes.[2] For improving the hole carrier injection characteristics, various hole injection layers (HILs) have been introduced, such as poly(3,4-ethylenedioxythiophene):poly(styrene sulfonate) (PEDOT:PSS), nanocarbon materials,[15] and transition metal oxides. Although the PEDOT:PSS is most widely used as an HIL in organic optoelectronic applications,[16] it suffers from chemical stability issues owing to its acidic nature and relatively limited Φ of 5.0−5.1 eV, which could cause a severe charge injection problem when organic materials with high ionization energy (>5.5 eV) are used. Alternatively, transition metal oxides, such as molybdenum or tungsten trioxide (MoO_3, WO_3), copper oxide (CuO), nickel oxide (NiO), and vanadium pentoxide (V_2O_5), have been introduced, and they exhibited superior device performance than the PEDOT:PSS in organic light-emitting diodes and organic photovoltaic cells.[17−21] Similarly, the S/D contact resistance in OFET can be greatly reduced by incorporating the transition metal oxides.[18,22−24] Although there has been remarkable progress to realize low-cost organic electronics, it is still not enough to predict the improvement of the injection characteristics in OFETs with low-cost metal electrodes because the exact charge injection mechanism through the transition metal oxide interlayers is not yet completely understood.

In this study, we report the fabrication of high-performance p-type polymer OFETs with Mo electrodes using a V_2O_5 interlayer. A thermally deposited V_2O_5 interlayer is formed between a regioregular poly(3-hexylthiophene) (rr-P3HT) or p-type polymer semiconductor containing dodecyl-substituted thienylenevinylene (TV) and dodecylthiophene (PC12TV12T) and the Mo source/drain electrode. The P3HT or PC12TV12T OFETs with the bare Mo electrode exhibited lower charge carrier mobility than those with Au because of a large barrier height for hole injection (0.5−1.0 eV). By forming the V_2O_5 layer, the P3HT or PC12TV12T OFETs with V_2O_5 on the Mo electrode exhibited charge carrier mobility comparable to that of a pristine Au electrode. The V_2O_5-deposited Mo exhibits comparable R_c to Au, which mainly resulted from the decreased barrier height for hole carrier injection from the low-cost Mo electrode to the frontier molecular orbital of the p-type polymer semiconductor after the incorporation of the transition metal oxide hole injection layer, such as V_2O_5.

2. METHODS

Field-Effect Transistor Fabrication. An OFET with a top-gate/bottom-contact (TG/BC) structure is fabricated on a glass substrate. After the conventional photolithography process of developing a photoresist layer for defining the source/drain patterns, a ∼3 nm thick Ti adhesion layer and ∼20 nm thick Mo electrodes are deposited by sputtering the Mo target on the Corning Eagle 2000 glass substrate, followed by lift-off of the photoresist layer. The source/drain electrodes are of various channel lengths (L) of 2, 5, 10, or 20 μm with a 1 mm channel width (W). The Mo/Ti electrode patterned substrates are cleaned sequentially in an ultrasonic bath with deionized water, acetone, and iso-propanol for 10 min each. A 1 or 5 nm thick V_2O_5 interlayer is deposited via thermal evaporation on a precleaned substrate. A p-type polymer semiconductor, rr-P3HT, is purchased from Sigma-Aldrich and a PC12TV12T is chemically synthesized using a previously published procedure[25] and dissolved in anhydrous chlorobenzene (CB) to obtain ∼10 mg/mL concentration solution. The solution is spin-coated on a V_2O_5 interlayer-deposited substrate and sequentially thermal annealed at 150 °C (for P3HT) or 200 °C (for PC12TV12T) for ∼30 min in nitrogen (N_2)-filled glovebox. A polymer dielectric layer, poly(methyl methacrylate) (PMMA), is purchased from Sigma-Aldrich, used without further purification, and dissolved in n-butylacetate (nBA) at 80 mg/mL concentration. A PMMA thin film is formed on the p-type polymer semiconductor layer by a spin-coating method, followed by thermal annealing at 80 °C for ∼30 min in the same N_2-filled glovebox to remove the residual solvents. The OFET device fabrication is completed by depositing the aluminum (Al) top-gate electrodes (∼50 nm thick) via thermal evaporation using a metal shadow mask.

Characterization. The surface morphology of the thin film is investigated using a tapping-mode atomic force microscope (AFM) (Nanoscope III, Veeco Instruments, Inc.) at the Korea Basic Science Institute (KBSI). X-ray photoemission spectroscopy (XPS) and ultraviolet photoemission spectroscopy (UPS) are measured using

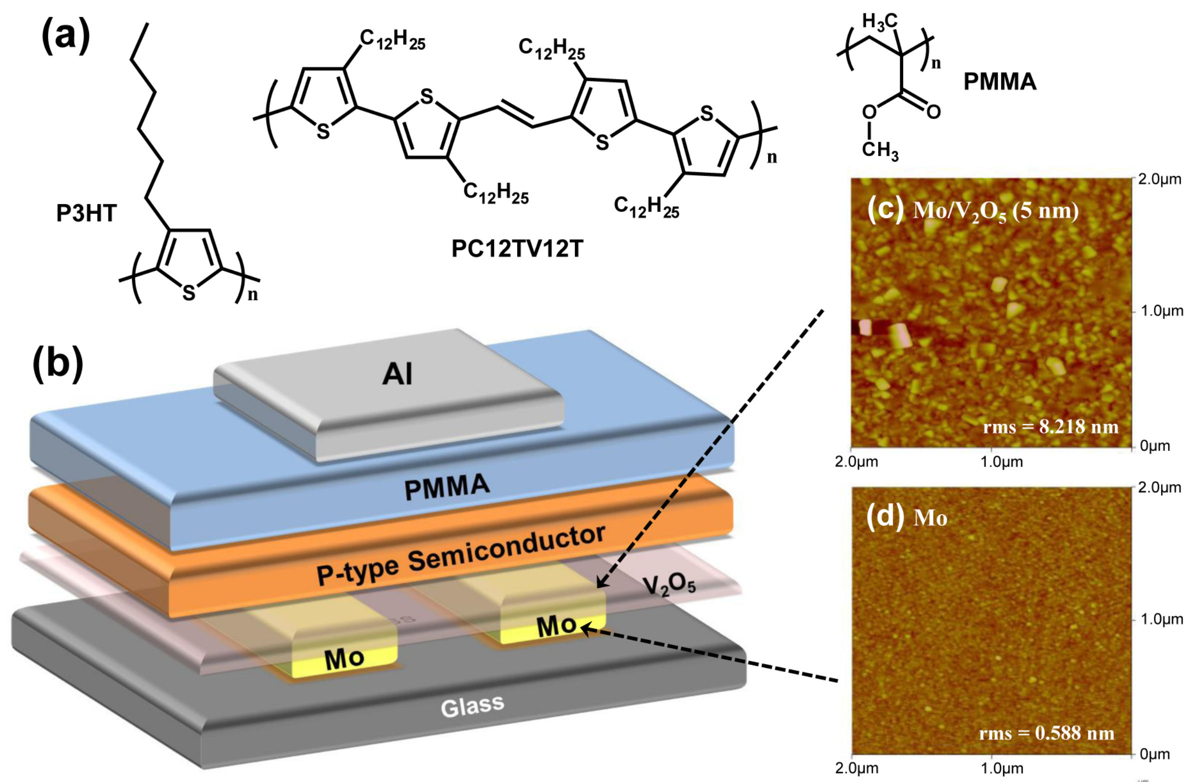

Figure 1. (a) Chemical structures of the p-type polymer semiconductors (rr-P3HT and PC12TV12T) and PMMA gate dielectric. (b) Top-gate/bottom-contact (TG/BC) OFET structure. (c, d) Tapping-mode AFM images of the (c) V_2O_5-deposited Mo and (d) pristine Mo electrodes.

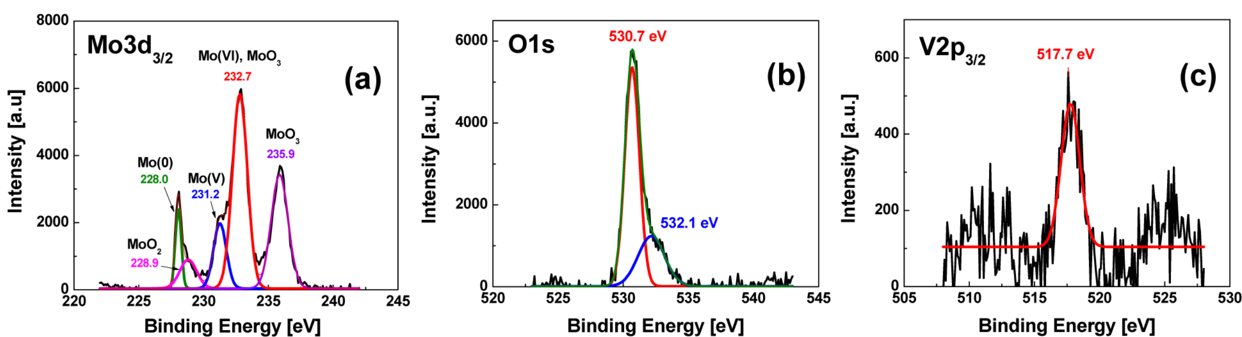

Figure 2. X-ray photoemission spectra for V_2O_5-deposited Mo electrodes: (a) Mo3d, (b) O1s, and (c) V2p core levels at room temperature.

AXIS-NOVA (Kratos, Inc.), with a base pressure of 4.2×10^{-9} Torr. The fundamental OFET electrical characteristics are measured using a Keithley 4200 semiconductor characterization system in N_2-filled glovebox. The conventional field-effect mobility (μ_{FET}) and corresponding V_{Th} are calculated at the saturation region (at a drain voltage V_d of −80 V) using gradual channel approximation equations for a standard metal oxide semiconductor FET (MOSFET).[26] The direct evaluation of the low-field mobility (μ_o) and R_c of the individual transistors is performed by the Y-function method (YFM), as described by Xu et al.[27]

3. RESULTS AND DISCUSSION

As shown in Figure 1, the OFET with a TG/BC structure is fabricated on a glass substrate. After the photolithography process for defining the Mo source/drain electrodes, the V_2O_5 interlayer is deposited onto the Mo electrode via thermal evaporation under high vacuum condition. Images c and d in Figure 1 show the tapping-mode AFM images of the V_2O_5-deposited and pristine Mo electrode surfaces, respectively. The pristine Mo electrode has a very uniform and flat surface topology with a root-mean-square roughness (R_q) of ∼0.558 nm. By contrast, the V_2O_5 layer thermally deposited on the Mo electrode increases the surface roughness, $R_q \approx 8.218$ nm, and submicrometer size V_2O_5 crystallites are formed on the electrode surface, as shown in Figure 1c. Although V_2O_5 leads to an increased surface roughness of both the contact electrodes and the active channel region between the source and the drain electrodes, the overall electrode surface is uniformly covered by a ∼5 nm thick transition metal oxide interlayer in order to modulate the charge injection properties of the uniform surface. Notably, the increased roughness of the channel region does not significantly affect the OFET performance, because the charge carrier transport in the top-gated OFET is mostly carried out on the top surface of the semiconductor layer. Figure 2 shows the X-ray photoemission spectra of the V_2O_5-deposited Mo electrodes, where the binding energies (E_B) are referenced to the residual hydrocarbon contamination at 284.9 ± 0.1 eV. The $Mo3d_{3/2}$ peaks at $E_B \approx$ 228.0, 228.9, 231.2, 232.7, and 235.9 eV, as shown in

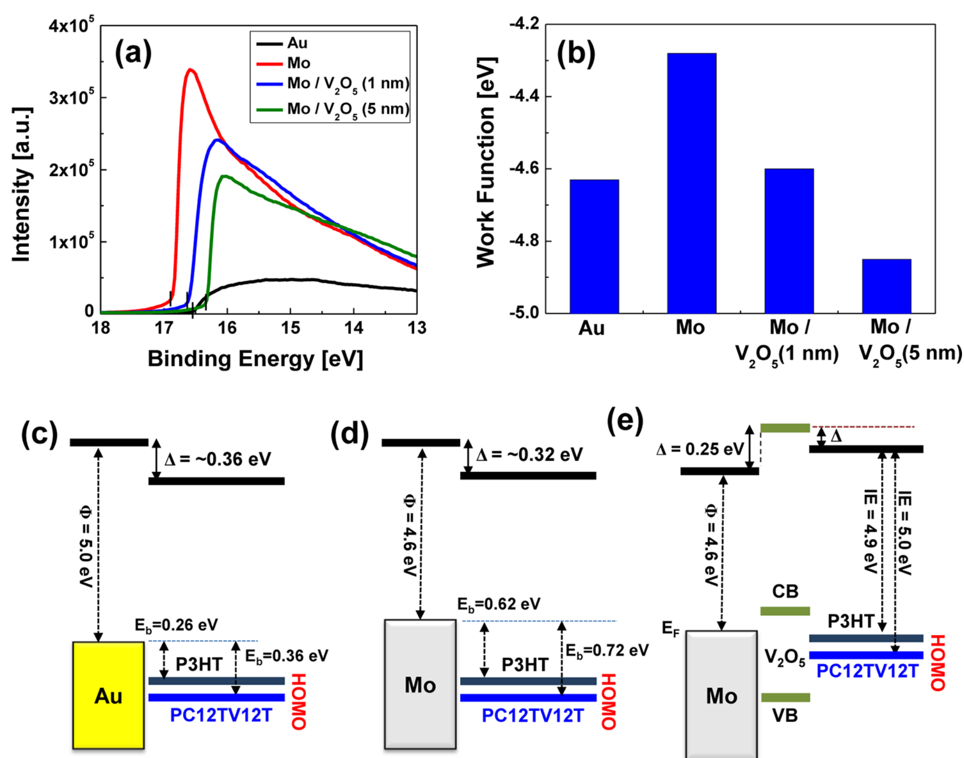

Figure 3. (a) Ultraviolet photoemission spectra of various metal electrodes; Au, Mo, and V_2O_5-deposited (1 nm or 5 nm thick) Mo electrodes and (b) work function of the corresponding metal electrodes. (c−e) Schematic energy diagrams of the charge injection from (c) pristine Au or (d) pristine Mo and (e) V_2O_5-incorporated Mo source/drain electrodes.

Figure 2a, correspond to Mo(0), MoO_2, Mo(V), Mo(VI)/MoO_3, and MoO_3, respectively.[28] It is observed that the pristine Mo surface consists of metallic Mo and native oxides (MoO_x), which might have formed during the photolithography process and by short exposure to air. As shown in Figure 2b, the oxygen signal at $E_B(\mathrm{O1s_A}) \approx 530.7$ eV corresponds to the oxygen ions of the V_2O_5 oxide layer, and the peak at $E_B(\mathrm{O1s_B}) \approx 532.1$ eV could be attributed either to the oxidation states of MoO_3 or to surface contamination.[29] For the V_2O_5 thin film on the Mo electrode, the E_B of the $V2p_{3/2}$core level is ∼517.7 eV, which is mainly related to the V^{5+} oxidation state, in agreement with the previously reported value.[30] Therefore, it can be concluded that the V_2O_5-deposited Mo electrode consists of mostly metallic Mo components and its native oxides (MoO_2 and MoO_3) and the thermally deposited V_2O_5 interlayer.

Figure 3 shows the ultraviolet photoemission spectra of the pristine Au and Mo, and the V_2O_5-deposited (1 or 5 nm thick) Mo electrodes and the corresponding values of Φ are shown in Figure 3b. Φ can be calculated from the UPS spectra by using the following eq 2

$$\phi = h\nu(= 21.2eV) - E_{\mathrm{cutoff}} + E_{\mathrm{Fermi}} \quad (2)$$

where E_{cutoff} and E_{Fermi} are the secondary electron cutoff and Fermi level, respectively. Although pure Au and Mo metals are known to have Φ values of ∼5.0 and ∼4.6 eV, respectively, those of pristine Au and Mo bottom-contact electrodes are ∼4.63 eV and ∼4.28 eV, respectively. This decreased Φ is mainly attributed to the interface dipoles (Δ) formed by the organic molecules adsorbed onto the clean metal surfaces presumably during the photolithography and wet-cleaning procedure. The interface dipoles are estimated to be ∼0.36 and ∼0.32 eV for Au and Mo electrodes, respectively, which leads to shifts in the photoemission onset toward the higher binding energy and a downward shift of the vacuum levels of the organic semiconductors. It can be noted that the naturally impure metal electrodes typically cause an increased barrier height (E_b) for hole carrier injection from the metal electrode to the frontier molecular orbital (i.e., HOMO) of the active semiconductor layer, despite being favorable for electron injection in the lowest unoccupied molecular orbital (LUMO) of the n-type or ambipolar semiconductors.[31,32] Although a metal electrode with a high Φ, such as Au, has inherently well-matched energy levels to form an Ohmic contact, this interface dipole typically causes a large charge injection barrier. In the case of Au, the barrier height (E_b) of ∼0.26 eV (∼0.36 eV) for hole carrier injection is not severe when compared with that of Mo, which has ∼0.62 eV (∼0.72 eV) for rr-P3HT [PC12TV12T] OFETs. Therefore, this large charge injection barrier height of greater than 0.6 eV with a relatively lower Φ of the Mo electrode when compared with Au can lead to increased R_c, thereby degrading the performance of the OFETs by decreasing μ_{app}.

In contrast to the pristine bottom-contact electrodes, the deposition of small amounts (1 and 5 nm thick) of V_2O_5 leads to a shift in the photoemission onset toward the lower binding energy by 0.57 eV, which implies the formation of an interface dipole consistent with an upward shift of the vacuum level, as shown in Figure 3e.[33] Thus, the Mo electrode with an ∼1 nm thick V_2O_5 layer is recovered to its original Φ value of ∼4.6 eV, and a 5 nm thick V_2O_5 layer further increases the Φ value to ∼4.85 eV, which is higher than that of the pristine Au bottom-contact electrode. Although the exact electronic structure of V_2O_5 and the resulting charge injection mechanism remain unclear, it has been reported that the valence band of V_2O_5 has

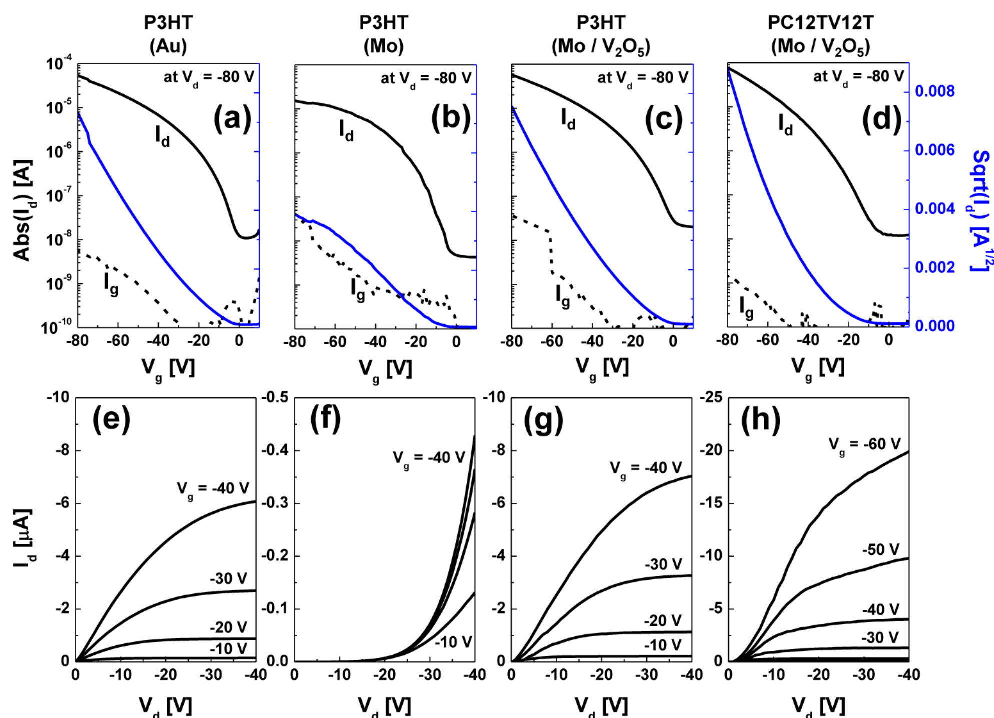

Figure 4. (a–d) Transfer (I_d vs V_g) and output (I_d vs V_d) characteristics of the OFETs with the p-type polymer semiconductors, P3HT or PC12TV12T, and various metal electrodes; (a, e) P3HT OFETs with pristine Au source/drain electrodes, (b, f) P3HT OFETs with pristine Mo electrodes, (c, g) P3HT OFETs with V_2O_5-deposited Mo electrodes, and (d, h) PC12TV12T OFETs with V_2O_5-deposited Mo electrodes.

Table 1. Fundamental Device Parameters of the P3HT and PC12TV12T OFETs with Various Metal Electrodes: Pristine Au or Mo and 5-nm-Thick V_2O_5-Deposited Mo Electrodes[a]

semiconductor	electrodes	thermal annealing	μ_{FET} (cm^2/(V s))	V_{Th} (V)	I_{on}/I_{off}	SS (V/dec)
P3HT	Au	150 °C for 30 min	0.14 ± 0.05	−30.3 ± 3	~1 × 10^4	−25.5
	Mo		0.02 ± 0.01	−11.1 ± 2	~1 × 10^3	−16.8
	Mo/V_2O_5 (~5 nm)		0.12 ± 0.05	−26.0 ± 3	~1 × 10^4	−27.3
PC12TVT12T	Au	200 °C for 30 min	0.40 ± 0.02	−26.2 ± 2	~1 × 10^4	−17.7
	Mo		0.27 ± 0.02	−36.8 ± 2	~1 × 10^3	−29.2
	Mo/V_2O_5 (~5 nm)		0.38 ± 0.03	−42.0 ± 2	~1 × 10^4	−26.8

[a]The field-effect mobility (μ_{FET}) and V_{Th} are obtained from the gradual channel approximation at the saturation region (at V_d = −80 V), W/L = 1.0 mm/20 μm, and dielectric capacitance per unit area (C_i) is ~6.2 nF/cm^2.

an ~5.5 eV width and a narrow conduction band of ~0.45 eV width, which is separated from the broad higher conduction band by an additional gap of ~0.35 eV.[34] These conduction and valence bands are separated by an indirect optical band gap, whose calculated band gap is ~1.74 eV (experimental value is ~2.2 eV).[34] Moreover, Kahn et al. reported that the electron affinity (EA), ionization potential (IE), and Φ of the V_2O_5 films were found to be equal to ~6.7, 9.5, and 7.0 eV, respectively.[33] When the V_2O_5 layer has such a high EA, the Fermi level (E_F) is nearly pinned against the conduction band minimum and is highly n-doped similar to MoO_3 and WO_3.[33] Therefore, it can be attributed that efficient hole injection can occur via electron extraction from the HOMO of the organic semiconductor to the minimum conduction band of the V_2O_5. Notably, the Φ value of the Mo electrode after the deposition of the V_2O_5 layer, in this study, is consistent with those of the other metal electrodes with the V_2O_5 layer (4.7−5.3 eV);[35−38] however, there are much smaller shifts (~0.57 eV) in the photoemission onset, as shown in Figure 3a, after incorporating the 5 nm thick V_2O_5 film. The amount of shift is obviously different from that of ~2.5 eV in the previous report by Kahn et al.; however, it is mostly attributed to the effect by air exposure of the freshly evaporated V_2O_5 film and contamination during the deposition of the polymer semiconductors by the solution process.[33] Even after a short-time exposure to air (~1 min), the photoemission spectrum could shift by ~1.5 eV toward the lower binding energy and induce a widening of the band gap to ~3.6 eV, resulting in a decrease in the Φ value to 5.5 eV.[33]

Figure 4 shows the transfer and output characteristics of the OFET devices with the p-type polymer semiconductors (P3HT and PC12TV12T) formed on various metal electrodes: pristine Au, pristine Mo, and V_2O_5-deposited Mo. The fundamental device parameters, such as the charge carrier mobility at the saturation region (at V_d = −80 V), V_{Th}, on/off-current ratio (I_{on}/I_{off}), subthreshold swing (SS), are listed in Table 1. For P3HT OFETs, the pristine Au electrode achieves relatively high hole mobilities of ~0.14 cm^2/(V s). Moreover, no significant nonlinear behavior in the output plots is observed at low V_d. In contrast to an Au electrode, a bare Mo electrode leads to superlinear output characteristics as shown in Figure 4f, which mostly resulted from large R_c between the charge injection electrode and the semiconductor active channel, and the

Table 2. Summary of the Parameters Extracted from the Conventional Field-Effect Mobility (μ_o) and from YFM for PC12TV12T OFETs with Au or V_2O_5-Deposited Mo (Mo/V_2O_5) Electrodes[a]

devices				conventional		YFM			
contact	W/L (μm)	V_d (V)	C_i (F/cm^2)	μ_{FET} (cm^2/(V s))	V_{Th} (V)	μ_o (cm^2/(V s))	V_{Th} (V)	θ (1/V)	R_cW (Ω cm)
Au	1000/2	−0.5	6.20×10^{-9}	6.40×10^{-5}	12.08	2.64×10^{-4}	−0.98	0.072	8.78×10^{6}
		−1.0		1.43×10^{-4}	9.46	3.55×10^{-4}	−3.03	0.033	3.02×10^{6}
	1000/5	−0.5		1.82×10^{-3}	−13.96	9.26×10^{-4}	−2.32	−0.066	5.71×10^{6}
		−1.0		3.42×10^{-3}	−18.85	1.24×10^{-3}	−16.75	−0.016	1.03×10^{6}
	1000/10	−0.5		2.49×10^{-3}	−24.37	1.22×10^{-3}	−1.27	−0.011	1.41×10^{6}
		−1.0		3.63×10^{-3}	−50.65	2.62×10^{-3}	−62.10	−0.020	1.25×10^{6}
	1000/20	−0.5		3.41×10^{-3}	−0.11	7.92×10^{-3}	−5.78	0.034	1.39×10^{6}
		−1.0		6.87×10^{-3}	−6.98	4.03×10^{-3}	−4.65	−0.017	1.33×10^{6}
Mo/V_2O_5	1000/2	−0.5		5.80×10^{-5}	18.49	1.09×10^{-3}	−20.39	−0.047	1.39×10^{6}
		−1.0		1.12×10^{-3}	−34.94	5.13×10^{-4}	−28.37	−0.017	1.09×10^{6}
	1000/5	−0.5		2.18×10^{-3}	−28.85	1.21×10^{-4}	−26.90	0.030	1.96×10^{6}
		−1.0		8.15×10^{-4}	−1.36	1.25×10^{-3}	−5.51	0.030	1.93×10^{6}
	1000/10	−0.5		5.66×10^{-4}	0.32	1.08×10^{-3}	−42.44	−0.014	2.12×10^{6}
		−1.0		6.93×10^{-3}	−39.44	5.45×10^{-3}	−37.71	−0.015	4.33×10^{5}
	1000/20	−0.5		1.22×10^{-2}	−34.56	7.53×10^{-3}	−31.45	−0.014	5.99×10^{5}
		−1.0		1.99×10^{-3}	−0.27	4.64×10^{-3}	−43.13	−0.015	1.07×10^{6}

[a] C_i is the dielectric capacitance per unit area, μ_o is the low-field mobility, V_{Th} is the threshold voltage, θ is the mobility attenuation factor, and R_cW is the width-normalized contact resistance with W = 1.0 mm).

corresponding hole mobilities are also remarkably degraded to ~0.02 cm^2/(V s) for the P3HT OFETs. It can be noted that the bottom-contact bare Mo electrode has a high barrier height of ~0.62 eV for hole injection from the Mo electrode to the HOMO of the P3HT. The large barrier height obviously increases R_c, causing a decrease in the μ_{app} of the OFETs. Importantly, the V_2O_5 thin film interlayer between the p-type polymer semiconductors and the Mo electrode effectively reduces the barrier height for charge carrier injection and decreases R_c such that the OFET performance is remarkably improved when compared with the devices with a pristine Au electrode. The hole mobility of the P3HT OFETs with the V_2O_5-deposited Mo electrode is about 0.12 cm^2/(V s). Similarly, PC12TV12T OFETs with Mo source/drain electrode also showed a recovery of hole mobility comparable to its pristine Au devices after inserting the V_2O_5 interlayer from 0.27 cm^2/(V s) to 0.38 cm^2/(V s).

R_c of the individual OFETs is evaluated by the YFM,[27] which is considered as a fast and precise alternative method for obtaining R_c when compared with the traditional transmission line method (TLM). From the transfer characteristics of the OFETs, I_d in the linear regime can be described as in eq 3

$$I_d = \frac{W}{L} C_i (V_g - V_{Th}) \frac{\mu_o}{1 + \theta(V_g - V_{Th})} V_d \quad (3)$$

where C_i is the dielectric capacitance per unit area, and μ_o is the low-field mobility. θ is the mobility attenuation factor, which consists of the extrinsic factors caused by the surface roughness and phonon scattering (θ_o) and contact resistance [$\theta^* = (W/L)\mu_o C_i R_c$]. Assuming a constant R_c, the transconductance (g_m) can be expressed as

$$g_m = \left.\frac{\partial I_d}{\partial V_g}\right|_{V_d = \text{const}} = \frac{W}{L} C_i \frac{\mu_o}{[1 + \theta(V_g - V_{Th})]^2} V_d \quad (4)$$

θ can be obtained by plotting $1/g_m^{1/2}$ versus V_g at a strong charge accumulation, where a linear behavior is obtained. Assuming that θ_o is negligible, R_c can be calculated, as summarized in Table 2. It can be noted that the negative value of θ, as summarized in Table 2, is presumably because of the gate-field enhanced mobility,[39] which is compensated for by the conventional mobility attenuation. The YFM enables us to precisely obtain the R_c of the individual transistors with the bare Au or V_2O_5-deposited Mo electrodes, in contrast to the TLM, by which only the average R_c value of the entire set of OFETs can be obtained. As shown in Figure 5, values of the channel width normalized contact resistance (R_cW) of the PC12TV12T OFETs with the bare Au and 5 nm thick V_2O_5 layer-deposited Mo electrode (Mo/V_2O_5) are similar, i.e., ~1×10^6 Ω cm. Notably, the Mo/V_2O_5 devices exhibited lower R_cW at shorter L below 10 μm in comparison with the PC12TV12T OFETs with a pristine Au electrode, as shown in Figure 5. However, it is mostly considered as deviation from the average value because the R_c is the resistance between the source/drain contact electrode and semiconductor active layer thus it would be independent of the L. Relatively large R_c values for the PC12TV12T OFETs even with staggered device structure is

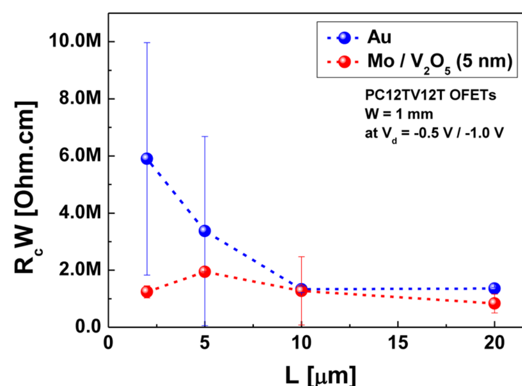

Figure 5. Channel width normalized contact resistance (R_cW) of the PC12TV12T OFETs with pristine Au or 5 nm thick V_2O_5-deposited Mo electrodes (Mo/V_2O_5), at different channel lengths (L) from 20 to 2 μm. The R_c is evaluated by YFM at low V_d of −0.5 or −1.0 V.

mainly attributed to characteristic feature of the PC12TV12T polymer semiconductor device rather than itself of Mo or Mo/V_2O_5 contact electrode, since Au electrode also showed similar nonlinear behavior in low V_d region compared to relatively linear slope of the P3HT devices, as can be seen in Figure 4 and Figure S1 in the Supporting Information. Although slightly higher (~0.1 eV) HOMO level of the PC12TV12T compared to that of the P3HT, PC12TV12T exhibited much larger R_c because of more deep frontier molecular orbital than estimated value by electrochemical analysis, cyclovoltametry,[25] and/or unfavorable molecular packing for charge injection from bottom-contact electrode. As the Φ of V_2O_5-deposited Mo electrode has relatively low value of ~4.85 eV, which presumably leads to still large charge injection barrier.

In conclusion, we have demonstrated high-performance polymer OFETs with a low-cost Mo source/drain electrode by efficient charge injection through the formation of a thermally deposited V_2O_5 thin film interlayer. The OFETs with the V_2O_5-deposited Mo electrode exhibited device performance comparable to that of the pristine Au electrode. This mainly results from the decreased barrier height for hole carrier injection from the low-cost metal electrode to the frontier molecular orbital of the p-type polymer semiconductor after the incorporation of the transition metal oxide HIL layer, such as V_2O_5. This enables the development of large-area, low-cost electronics with the Mo electrodes and V_2O_5 interlayer.

■ ASSOCIATED CONTENT

Supporting Information

Transfer and output characteristics of PC12TV12T OFETs with pristine Au, pristine Mo, and V_2O_5-deposited Mo source/drain electrodes. This material is available free of charge via the Internet at http://pubs.acs.org/.

■ AUTHOR INFORMATION

Corresponding Author

*E-mail: yynoh@dongguk.edu.

Notes

The authors declare no competing financial interest.

■ ACKNOWLEDGMENTS

This work was financially supported by the Dongguk University Research Fund of 2013; the Basic Science Research Program through the National Research Foundation of Korea (NRF), funded by the Ministry of Education, Science and Technology (MEST) (2010-0023180); a grant (13-12-N0101-41) from the Primary Research Program of Korea Electrotechnology Research Institute (KERI). The authors appreciate to prof. D.-Y. Kim and J. Kim for supplying the p-type semiconductor, PC12TV12T.

■ REFERENCES

(1) Klauk, H. *Chem. Soc. Rev.* **2010**, *39*, 2643−2666.
(2) Natali, D.; Caironi, M. *Adv. Mater.* **2012**, *24*, 1357−1387.
(3) Facchetti, A.; Yoon, M. H.; Marks, T. J. *Adv. Mater.* **2005**, *17*, 1705−1725.
(4) Søndergaard, R. R.; Hosel, M.; Krebs, F. C. *J. Polym. Sci., Part B: Polym. Phys.* **2012**, *51*, 16−34.
(5) Chen, Z. Y.; Lee, M. J.; Ashraf, R. S.; Gu, Y.; Albert-Seifried, S.; Nielsen, M. M.; Schroeder, B.; Anthopoulos, T. D.; Heeney, M.; McCulloch, I.; Sirringhaus, H. *Adv. Mater.* **2012**, *24*, 647−652.
(6) Lee, J.; Han, A.-R.; Kim, J.; Kim, Y.; Oh, J. H.; Yang, C. *J. Am. Chem. Soc.* **2012**, *134*, 20713−20721.
(7) Li, J.; Zhao, Y.; Tan, H. S.; Guo, Y.; Di, C.-A.; Yu, G.; Liu, Y.; Lin, M.; Lim, S. H.; Zhou, Y.; Su, H.; Ong, B. S. *Sci. Rep.* **2012**, *2*, 754.
(8) Ante, F.; Kalblein, D.; Zaki, T.; Zschieschang, U.; Takimiya, K.; Ikeda, M.; Sekitani, T.; Someya, T.; Burghartz, J. N.; Kern, K.; Klauk, H. *Small* **2012**, *8*, 73−79.
(9) Benor, A.; Knipp, D. *Org. Electron.* **2008**, *9*, 209−219.
(10) Rhee, S.-W.; Yun, D.-J. *J. Mater. Chem.* **2008**, *18*, 5437−5444.
(11) Sele, C. W.; von Werne, T.; Friend, R. H.; Sirringhaus, H. *Adv. Mater.* **2005**, *17*, 997−1001.
(12) Aguirre, C. M.; Ternon, C.; Paillet, M.; Desjardins, P.; Martel, R. *Nano Lett.* **2009**, *9*, 1457−1461.
(13) Southard, A.; Sangwan, V.; Cheng, J.; Williams, E. D.; Fuhrer, M. S. *Org. Electron.* **2009**, *10*, 1556−1561.
(14) Zhang, Y. Y.; Shi, Y.; Chen, F.; Mhaisalkar, S. G.; Li, L.-J.; Ong, B. S.; Wu, Y. *Appl. Phys. Lett.* **2007**, *91*, 223512.
(15) Yun, J.-M.; Yeo, J.-S.; Kim, J.; Jeong, H.-G.; Kim, D.-Y.; Noh, Y.-J.; Kim, S.-S.; Ku, B.-C.; Na, S.-I. *Adv. Mater.* **2011**, *23*, 4923−4928.
(16) Heithecker, D.; Kammoun, A.; Dobbertin, T.; Riedl, T.; Becker, E.; Metzdorf, D.; Schneider, D.; Johannes, H.-H.; Kowalsky, W. *Appl. Phys. Lett.* **2003**, *82*, 4178−4180.
(17) Steirer, K. X.; Chesin, J. P.; Widjonarko, N. E.; Berry, J. J.; Miedaner, A.; Ginley, D. S.; Olson, D. C. *Org. Electron.* **2010**, *11*, 1414−1418.
(18) Chu, C.-W.; Li, S.-H.; Chen, C.-W.; Shrotriya, V.; Yang, Y. *Appl. Phys. Lett.* **2005**, *87*, 193508.
(19) Meyer, J.; Hamwi, S.; Bulow, T.; Johannes, H.-H.; Riedl, T.; Kowalsky, W. *Appl. Phys. Lett.* **2007**, *91*, 113506.
(20) Kanai, K.; Koizumi, K.; Ouchi, S.; Tsukamoto, Y.; Sakanoue, K.; Ouchi, Y.; Seki, K. *Org. Electron.* **2010**, *11*, 188−194.
(21) Park, J.-W.; Baeg, K.-J.; Ghim, J.; Kang, S.-J.; Park, J.-H.; Kim, D.-Y. *Electrochem. Solid-State Lett.* **2007**, *10*, H340−H343.
(22) Wang, W.; Ma, D.; Pan, S.; Yang, Y. *Appl. Phys. Lett.* **2012**, *101*, 033303.
(23) Kumaki, D.; Umeda, T.; Tokito, S. *Appl. Phys. Lett.* **2008**, *92*, 013301.
(24) Chan, C. Y. H.; Chow, C. M.; So, S. K. *Org. Electron.* **2011**, *12*, 1454−1458.
(25) Kim, J.; Lim, B.; Baeg, K.-J.; Noh, Y.-Y.; Khim, D.; Jeong, H.-G.; Yun, J.-M.; Kim, D.-Y. *Chem. Mater.* **2011**, *23*, 4663−4665.
(26) Sze, S. M.; Ng, K. K. *Physics of Semiconductor Devices*, 3rd ed.; Wiely−Interscience: Hoboken, NJ, 2007.
(27) Xu, Y.; Minari, T.; Tsukagoshi, K.; Chroboczek, J. A.; Ghibaudo, G. *J. Appl. Phys.* **2010**, *107*, 114507.
(28) Spevack, P. A.; McIntyre, N. S. *J. Phys. Chem.* **1993**, *97*, 11020−11030.
(29) Ibris, N.; Salvi, A. M.; Liberatore, M.; Decker, F.; Surca, A. *Surf. Interface Anal.* **2005**, *37*, 1092−1104.
(30) Lindström, R.; Maurice, V.; Zanna, S.; Klein, L.; Groult, H.; Perrigaud, L.; Cohen, C.; Marcus, P. *Surf. Interface Anal.* **2006**, *38*, 6−18.
(31) Yan, H.; Chen, Z. H.; Zheng, Y.; Newman, C.; Quinn, J. R.; Dotz, F.; Kastler, M.; Facchetti, A. *Nature* **2009**, *457*, 679−686.
(32) Baeg, K.-J.; Kim, J.; Khim, D.; Caironi, M.; Kim, D.-Y.; You, I.-K.; Quinn, J. R.; Facchetti, A.; Noh, Y.-Y. *ACS Appl. Mater. Interfaces* **2011**, *3*, 3205−14.
(33) Meyer, J.; Zilberberg, K.; Riedl, T.; Kahn, A. *J. Appl. Phys.* **2011**, *110*, 033710.
(34) Eyert, V.; Höck, K. H. *Phys. Rev. B* **1998**, *57*, 12727−12737.
(35) Wang, Z. B.; Helander, M. G.; Qiu, J.; Liu, Z. W.; Greiner, M. T.; Lu, Z. H. *J. Appl. Phys.* **2010**, *108*, 024510.
(36) Zhang, H. M.; Choy, W. C. H. *IEEE Trans. Electron Devices* **2008**, *55*, 2517−2520.
(37) Helander, M. G.; Wang, Z. B.; Greiner, M. T.; Qiu, J.; Lu, Z. H. *Appl. Phys. Lett.* **2009**, *95*, 083301.
(38) Shrotriya, V.; Li, G.; Yao, Y.; Chu, C.-W.; Yang, Y. *Appl. Phys. Lett.* **2006**, *88*, 073508.
(39) Horowitz, G.; Hajlaoui, R.; Fichou, D.; Kassmi, A. E. *J. Appl. Phys.* **1999**, *85*, 3202−3206.